

Article

New Multicolor Tungstate-Molybdate Microphosphors as an Alternative to LED Components

Justyna Czajka ¹ , Agata Szczeszak ^{2,*} , Nina Kaczorowska ² and Stefan Lis ²

¹ Faculty of Chemical Technology and Engineering, Bydgoszcz University of Science and Technology, Seminaryjna 3, 85-326 Bydgoszcz, Poland; justyna.czajka@pbs.edu.pl

² Faculty of Chemistry, Adam Mickiewicz University, Uniwersytetu Poznańskiego 8, 61-614 Poznań, Poland; nina.kaczorowska@amu.edu.pl (N.K.); blis@amu.edu.pl (S.L.)

* Correspondence: agata_is@amu.edu.pl; Tel.: +48-61-829-1777

Abstract: Due to the ongoing need to create phosphors with the appropriate emission color for the production of light emitting diodes, we decided to synthesize a series of multicolour microphosphors with tunable visible emissions, depending on the composition of dopant ions. In this work, we investigated the structure, morphology, and luminescent properties of new molybdate–tungstate phosphors co-doped with Tb³⁺ and Eu³⁺ ions. The conventional high temperature solid state method was used to prepare a series of CaMo_yW_{1-y}O₄:Eu³⁺_x/Tb³⁺_{1-x} materials. In order to obtain phosphors with the most promising luminescent properties, the experiment was planned by taking into account the different composition of the matrix and the concentration of the particular dopant ions (Eu³⁺_x/Tb³⁺_{1-x}, x = 0.001, 0.003, 0.005, 0.007, 0.009). As a result, luminescent materials were obtained with a pure tetragonal crystal structure, the space group of I₄₁/a, confirmed by X-ray diffraction (XRD). The size and shape of the particles obtained from the materials were analyzed based on scanning electron microscopy images. Luminescence spectroscopy (excitation and emission spectra, decay lifetimes) was utilized to characterize the luminescence properties of the as-prepared phosphors. The color change of the emission from green-yellow to orange-red was confirmed using the 1931 Commission Internationale de l’Eclairage (CIE) chromaticity coordinates and color correlated temperature (CCT).

Keywords: luminescence; LED components; lanthanides; optical materials; tungstate–molybdate phosphors



Citation: Czajka, J.; Szczeszak, A.; Kaczorowska, N.; Lis, S. New Multicolor Tungstate-Molybdate Microphosphors as an Alternative to LED Components. *Materials* **2021**, *14*, 6608. <https://doi.org/10.3390/ma14216608>

Academic Editors: Tao-Hsing Chen and Shih-Chen Shi

Received: 8 October 2021

Accepted: 27 October 2021

Published: 2 November 2021

Publisher’s Note: MDPI stays neutral with regard to jurisdictional claims in published maps and institutional affiliations.



Copyright: © 2021 by the authors. Licensee MDPI, Basel, Switzerland. This article is an open access article distributed under the terms and conditions of the Creative Commons Attribution (CC BY) license (<https://creativecommons.org/licenses/by/4.0/>).

1. Introduction

Recently, many investigations have focused on the synthesis and characterization of molybdate [1–5] and tungstate [6–10] materials with a tetragonal scheelite structure [11–13] doped with trivalent lanthanide ions, Ln³⁺. Many different synthesis methods including sol-gel [5,14,15], sonochemical methods [16,17], hydrothermal methods [18,19], microwave assisted hydrothermal routes [20,21] as well as high temperature solid state methods [22–24], have been used to improve the structural and physicochemical properties of the synthesized molybdate/tungstate materials [25]. Economic aspects [7], technological importance [26], and possible applications have also been taken into account [7,27]. Inorganic luminescent materials doped with Ln³⁺ ions are well known as phosphors that are applied, for example, in solar cells [28,29], scintillators, light emitting diodes [30], lasers [31], bioimaging [14], and field emission displays [24]. Designing modern tunable luminescent materials with a wide range of applications has been a global trend for several years. Due to the rapid development of knowledge in the field of synthesis and properties of luminescent modern phosphors consisting of Ln³⁺ ions and tungstate or molybdate matrices, we decided to present new tunable phosphors based on mixed inorganic matrices.

In this work, studies of the structure, morphology, and luminescence properties were carried out using different compositions of terbium, Tb³⁺, and europium, Eu³⁺,

dopant ions, as well as with a different composition of the matrix (different W/Mo ratio) synthesized by the high temperature solid state method. Several techniques were used to characterize as-synthesized phosphors, including using X-ray powder diffraction, scanning electron microscopy, and photoluminescence spectroscopy, respectively. Under the selected excitation wavelength, Tb^{3+} and Eu^{3+} ions emit light with a color ranging from green through orange to red. Therefore, the synthesized phosphors have potential in an LED application. In this study, the correlated color temperature was calculated and the color emission was visualized on chromaticity diagrams and schemes.

The most recent articles describing materials for LEDs show that there remains a need for phosphors for the production of efficient and bright lighting LEDs [32] that are also produced based on a high temperature solid state reaction [33–36]. In fact, the literature reports extensive research on molybdate and tungstate matrices doped with Eu^{3+} [33,37,38] or Tb^{3+} ions [39,40]; however, the materials of the composition studied in the presented manuscript have not yet been investigated. Therefore, we present detailed studies of $CaMo_yW_{1-y}O_4:Eu^{3+}_x/Tb^{3+}_{1-x}$ materials. The literature also provides information on tunable fluoride materials doped with Eu^{3+} and Tb^{3+} [41] or lithium borate glasses doped with Eu^{3+} and Tb^{3+} [42], which indicates the importance of the Eu^{3+}/Tb^{3+} ion dopant system in the creation of novel lighting setups.

The presented manuscript shows Eu^{3+}/Tb^{3+} -doped phosphors based on a mixed matrix, the luminescent properties of which are controlled by the matrix composition, as well as the number of dopant ions. As a result, the effects on changes in the correlated color temperature (CCT) and chromaticity parameters are analyzed in detail. According to our knowledge, such detailed data are not known in the literature.

2. Materials and Methods

$CaMo_yW_{1-y}O_4:Eu^{3+}_x/Tb^{3+}_{1-x}$ phosphors were synthesized by the traditional solid state reaction method. The complete formula used for the required calculations is $Ca_{0.99}Mo_yW_{1-y}O_4:Eu^{3+}_x/Tb^{3+}_{1-x}$; however, for simplicity, the shorter version will be used in the text. In order to obtain materials exhibiting tunable intense emission, an experiment was planned regarding the matrix composition ($CaMo_yW_{1-y}O_4:Eu^{3+}_x/Tb^{3+}_{1-x}$) and the concentration of dopant ions as follows: $y = 0.1 - 0.9$, $x = 0.1 - 0.9$. The starting materials were purchased from Stanford Materials (Lake Forest, CA, USA) (europium oxide (Eu_2O_3 , 99.99%), terbium oxide (Tb_4O_7 , 99.99%)), Sigma Aldrich (molybdenum oxide (MoO_3 , 99.9%), tungsten oxide (WO_3 , 99.9%)) as well as from POCh Gliwice (calcium carbonate ($CaCO_3$, 99.5%)). In the first step, $CaCO_3$, MoO_3 , and WO_3 were mixed at a $1:y:1-y$ molar ratio ($y = 0.1 - 0.9$), while in the second step, appropriate amounts of Eu_2O_3 and Tb_4O_7 were added and the total molar concentration of activator (Eu^{3+}_x/Tb^{3+}_{1-x}) ions was 1 mol.% ($x = 0.001, 0.003, 0.005, 0.007, 0.009$). The starting materials were ground thoroughly in an agate mortar for 1 h. Finally, the obtained homogeneous powders were placed in corundum crucibles and sintered in a muffle furnace at 900 °C for 4 h. After the calcination process, the samples were cooled down to room temperature. The structure of the final products was determined by X-ray powder diffraction (XRD) (BRUKER D8 Advance, Karlsruhe, Germany) using Cu-K α radiation ($\lambda = 0.1541874$ nm), registered from 10° to 60° (2 θ) with the step of 0.05°. Scanning electron microscopy (SEM) images were obtained with the use of a HITACHI SU3500 equipped with a BSE-3D detector (Tokyo, Japan), using an acceleration voltage of 10.0 kV. Excitation and emission spectra were measured on a Hitachi F-7000 fluorescence spectrofluorimeter (Tokyo, Japan) and corrected for the light source used (xenon lamp). The CIE 1931 chromaticity coordinates, x and y , were used to determine CCT using the McCamy equation [43].

3. Results

As a result of the solid state reaction, a series of tunable $CaMo_yW_{1-y}O_4$ codoped with Eu^{3+} and Tb^{3+} ions was obtained. The representative composition of the matrix $CaMo_{0.5}W_{0.5}O_4$ was selected and it was used in further studies as the most suitable for the

introduction of dopant ions and for studying the dependency of Eu^{3+} and Tb^{3+} concentration on luminescence parameters. The influence of dopant ions on the structural properties of tungstate–molybdate matrices was analyzed based on XRD patterns for representative samples (Figure 1). The structure of the prepared materials can be indexed to a tetragonal crystal structure with the space group $I4_1/a$ of the scheelite type CaWO_4 referenced by card number 96-900-9628. The crystal structure agreed well with card number 96-900-9633 and also confirmed the tetragonal structure CaMoO_4 . Based on the consistency of the diffractograms with the reference pattern, no other phases and impurities were detected. It was confirmed that the introduction of Tb^{3+} and Eu^{3+} dopants did not disturb the structure, thanks to the Ln^{3+} ions which were successfully incorporated into the host lattice [25,44]. In the described structures, hexavalent M^{6+} ($\text{M} = \text{W}, \text{Mo}$) atoms coordinate with four O^{2-} atoms and divalent Ca^{2+} atoms coordinate with eight O^{2-} atoms, respectively [22,45]. The similarity in the ionic radii between W^{6+} (0.42 Å) and Mo^{6+} (0.41 Å) confirmed that the positions of the diffraction peaks hardly changed [24], while the pointed diffraction peaks of high amplitude confirmed the high crystallinity of the synthesized luminescent materials [22]. In addition, the similarity of the ionic radii of Eu^{3+} ($r = 1.07 \text{ \AA}$ for CN = 8) and Tb^{3+} ($r = 1.04 \text{ \AA}$ for CN = 8) with the ionic radius of Ca^{2+} ($r = 1.12 \text{ \AA}$ for CN = 8), and the purity of the samples, indicate that the lanthanide dopant ions are expected to substitute Ca^{2+} ions [6].

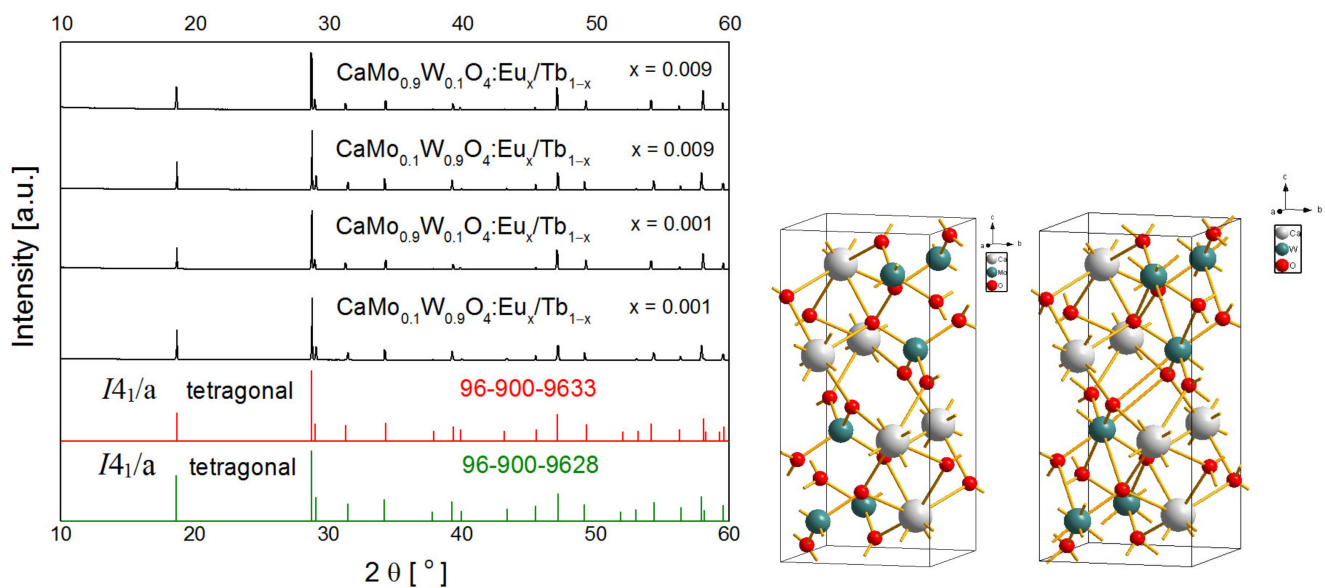


Figure 1. XRD patterns of $\text{CaMo}_{0.9}\text{W}_{0.1}\text{O}_4$ and $\text{CaMo}_{0.1}\text{W}_{0.9}\text{O}_4$ materials doped with $\text{Eu}^{3+}/\text{Tb}^{3+}_{1-x}$ ($x = 0.001$, $x = 0.009$), synthesized at $900 \text{ }^\circ\text{C}$ for 4 h.

The scanning electron microscopy (SEM) images shown in Figure 2 present the morphology of $\text{CaMo}_y\text{W}_{1-y}\text{O}_4:\text{Eu}^{3+}_x/\text{Tb}^{3+}_{1-x}$ luminescent materials synthesized by the high temperature solid state technique at $900 \text{ }^\circ\text{C}$ for 4 h. It is revealed that the samples have a topography typical for this method. Despite the tendency towards agglomeration [6,46], it was possible to estimate the average grain size, which covers the $0.5\text{--}12 \text{ }\mu\text{m}$ range. To be precise, most of the samples exhibited a grain size in the range of $0.5\text{--}3 \text{ }\mu\text{m}$. The results of these estimates are shown in the form of size distribution in Figure 2.

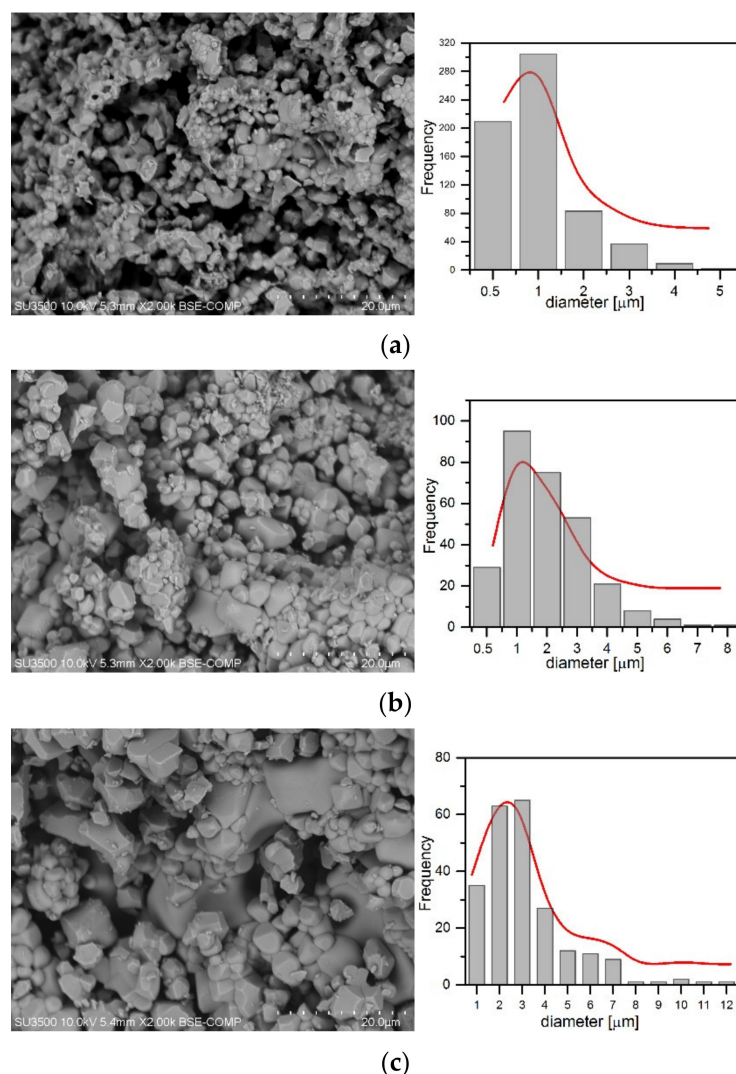


Figure 2. SEM images and histograms of samples (a) $\text{CaMo}_{0.5}\text{W}_{0.5}\text{O}_4:\text{Eu}^{3+}_{0.005}/\text{Tb}^{3+}_{0.005}$, (b) $\text{CaMo}_{0.9}\text{W}_{0.1}\text{O}_4:\text{Eu}^{3+}_{0.009}/\text{Tb}^{3+}_{0.001}$, (c) $\text{CaMo}_{0.1}\text{W}_{0.9}\text{O}_4:\text{Eu}^{3+}_{0.001}/\text{Tb}^{3+}_{0.009}$.

Figure 3 shows the excitation spectra of $\text{CaMo}_{0.5}\text{W}_{0.5}\text{O}_4:\text{Eu}^{3+}_x/\text{Tb}^{3+}_{1-x}$ measured at wavelengths corresponding to the most intense emission bands of Tb^{3+} ($\lambda_{\text{em}} = 546 \text{ nm}$, $^5\text{D}_4 \rightarrow ^7\text{F}_5$) and Eu^{3+} ($\lambda_{\text{em}} = 617 \text{ nm}$, assigned to $^5\text{D}_0 \rightarrow ^7\text{F}_2$). Both spectra present broad bands with maxima in the range of 200–350 nm, which is the result of the charge transfer (CT) phenomenon. These bands consist of the individual components such as the transitions $\text{O}^{2-} \rightarrow \text{W}^{6+}$, $\text{O}^{2-} \rightarrow \text{Mo}^{6+}$, $\text{O}^{2-} \rightarrow \text{Tb}^{3+}$, and $\text{O}^{2-} \rightarrow \text{Eu}^{3+}$. The intensity and broadness of the CT bands indicate the effectively activated emission of Eu^{3+} and Tb^{3+} ions through energy transfer between WO_4^{3-} and MoO_4^{3-} groups and activator ions, after CT between W^{6+} or Mo^{6+} and O^{2-} [24,47]. Moreover, in the excitation spectra, there are several weak absorption peaks of Eu^{3+} and Tb^{3+} (Figure 3a). The bands at 350, 358, 367, 377 and 486 nm are assigned to the 4f–5d transitions of Tb^{3+} from the ground level $^7\text{F}_6$ to the $^7\text{D}_2$, $^5\text{G}_5$, $^5\text{G}_6$, $^5\text{D}_3$ and $^5\text{D}_4$ excited levels of Tb^{3+} , whereas the peaks at 376 and 393 nm are ascribed to the 4f–4f transitions of Eu^{3+} from the ground level $^7\text{F}_0$ to the $^5\text{G}_2$ and $^5\text{L}_6$ excited levels of Eu^{3+} , respectively. The excitation spectra monitored at $\lambda_{\text{em}} = 617 \text{ nm}$ (Figure 3b) consist of 360 nm ($^7\text{F}_0 \rightarrow ^5\text{D}_4$), 375 nm ($^7\text{F}_0 \rightarrow ^5\text{G}_2$), 380 nm ($^7\text{F}_0 \rightarrow ^5\text{G}_3$), 393 nm ($^7\text{F}_0 \rightarrow ^5\text{L}_6$), 415 nm ($^7\text{F}_0 \rightarrow ^5\text{D}_3$), and 464 nm ($^7\text{F}_0 \rightarrow ^5\text{D}_2$) peaks, typical for Eu^{3+} . This means that we found the characteristic excitation from Eu^{3+} when monitoring the luminescence of Tb^{3+} (Figure 3a). On the other hand, when observing the Eu^{3+} luminescence, the characteristic peaks of Tb^{3+} are missing. This may indicate that the energy transfer from Eu^{3+} to Tb^{3+} is efficient.

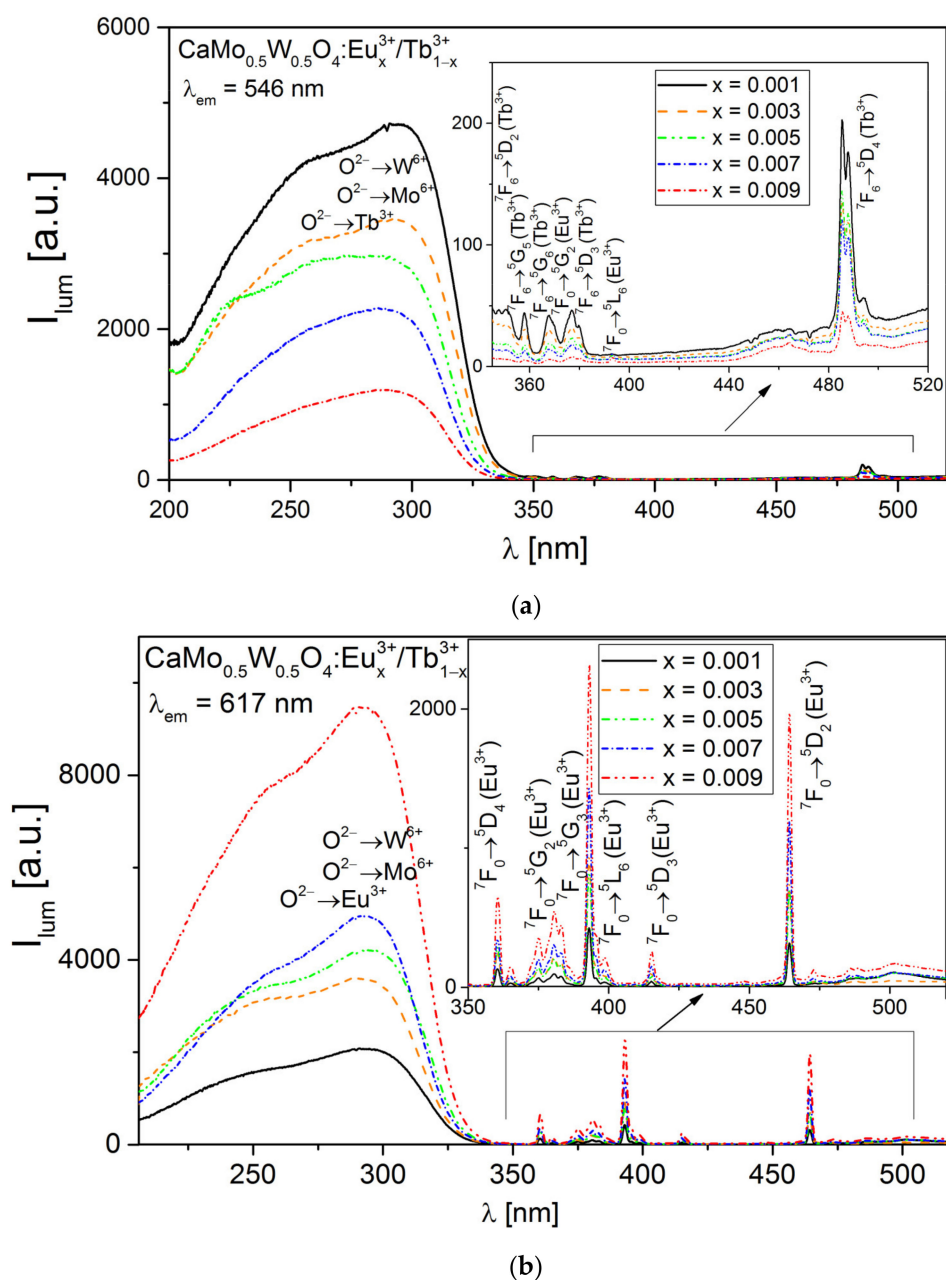


Figure 3. Excitation spectra of $\text{CaMo}_{0.5}\text{W}_{0.5}\text{O}_4:\text{Eu}^{3+}_x/\text{Tb}^{3+}_{1-x}$ phosphors monitored at a wavelength of (a) $\lambda_{\text{em}} = 546$ nm and (b) $\lambda_{\text{em}} = 617$ nm. The inserts magnify the bands in the range from 350 to 520 nm.

Figure 4 shows the emission spectra of $\text{CaMo}_{0.5}\text{W}_{0.5}\text{O}_4:\text{Eu}^{3+}_x/\text{Tb}^{3+}_{1-x}$ materials with excitation of 256 nm (a), 272 nm (b), and 394 nm (c). The emission spectra (Figure 4a,b) contain a wide range of bands from 400 to 600 nm assigned to the matrix emission, which indicates that the energy transfer from the host towards the dopant ions is not complete. Furthermore, it can be observed that its intensity decreases with an increasing amount of Eu^{3+} dopant ions. All samples show a strong emission at 617 nm and 546 nm upon 256 and 272 nm excitation. The emission peak at 617 nm is assigned to the ${}^5\text{D}_0 \rightarrow {}^7\text{F}_2$ electric dipole transition of Eu^{3+} , while the band at 546 nm is ascribed to the ${}^5\text{D}_4 \rightarrow {}^7\text{F}_5$ of Tb^{3+} . Other peaks are assigned at 490 nm (${}^5\text{D}_4 \rightarrow {}^7\text{F}_6$ of Tb^{3+}), 589 nm (${}^5\text{D}_4 \rightarrow {}^7\text{F}_5$, Tb^{3+}), 593 nm (${}^5\text{D}_0 \rightarrow {}^7\text{F}_1$, Eu^{3+}), 657 nm (${}^5\text{D}_0 \rightarrow {}^7\text{F}_3$, Eu^{3+}) and 705 nm (${}^5\text{D}_0 \rightarrow {}^7\text{F}_4$, Eu^{3+}). Apart from Eu^{3+} , under the excitation of 394 nm, there are also emission bands assigned to the Tb^{3+} ion. This may indicate effective energy transfer from Eu^{3+} to Tb^{3+} (Figure 5) [48].

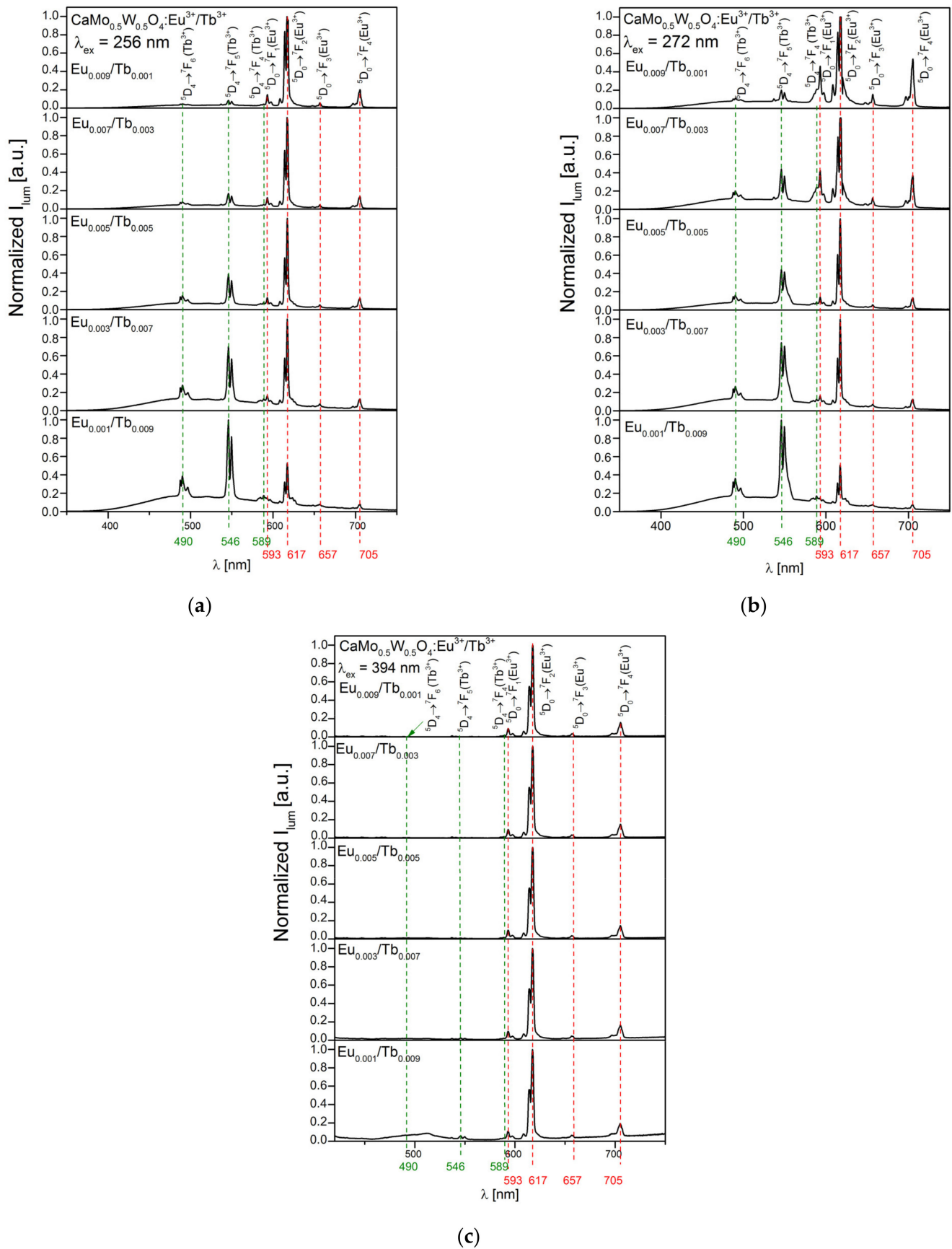


Figure 4. Emission spectra of $\text{CaMo}_{0.5}\text{W}_{0.5}\text{O}_4:\text{Eu}^{3+}_x/\text{Tb}^{3+}_{1-x}$ phosphors (a) $\lambda_{\text{ex}} = 256 \text{ nm}$, (b) $\lambda_{\text{ex}} = 272 \text{ nm}$, (c) $\lambda_{\text{ex}} = 394 \text{ nm}$.

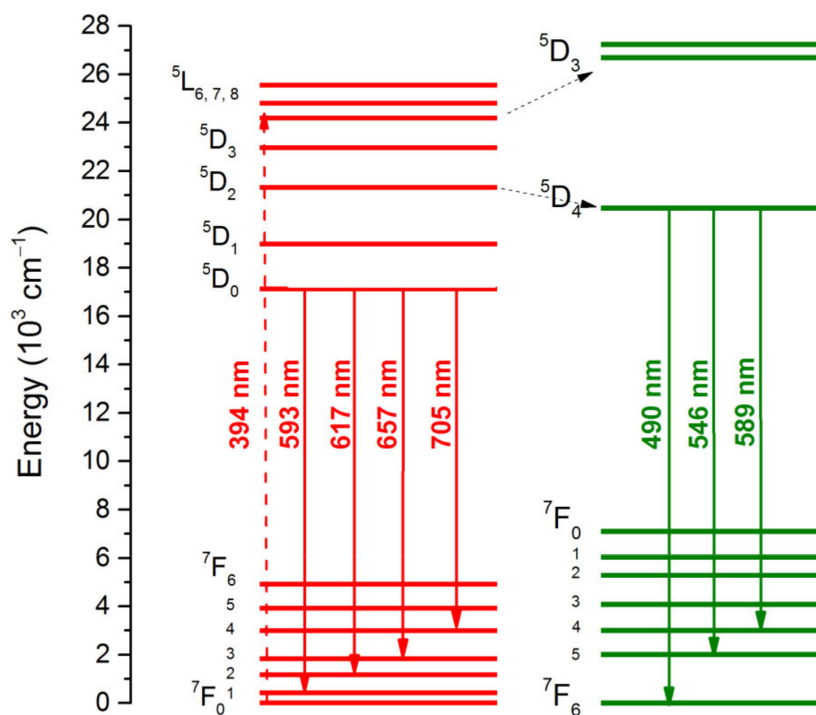


Figure 5. Energy level scheme diagram showing ET from Eu^{3+} to Tb^{3+} .

The decay curves of the Tb^{3+} transitions at 490 nm, 546 nm, and 589 nm in $\text{CaMo}_{0.5}\text{W}_{0.5}\text{O}_4:\text{Eu}^{3+}_x/\text{Tb}^{3+}_{1-x}$ phosphors were measured under the 256 nm excitation wavelength as represented in Figure 6a–c, respectively. The decay curves of Eu^{3+} were also measured under the 256 nm excitation wavelength for the emissions at 617 nm, 656 nm, and 705 nm, which correspond to the ${}^5\text{D}_0 \rightarrow {}^7\text{F}_2$, ${}^5\text{D}_0 \rightarrow {}^7\text{F}_3$, and ${}^5\text{D}_0 \rightarrow {}^7\text{F}_4$ transitions, respectively. All curves were fitted by one-exponential decay. To identify and analyze more detailed ET from Eu^{3+} to Tb^{3+} , we recorded decay curves under $\lambda_{\text{ex}} = 394$ nm (Figure 6g). The slightly longer lifetime of Tb^{3+} ($\lambda_{\text{em}} = 546$ nm) and shorter lifetime time of Eu^{3+} ($\lambda_{\text{em}} = 617$ nm) may indicate energy migration from Eu^{3+} to Tb^{3+} .

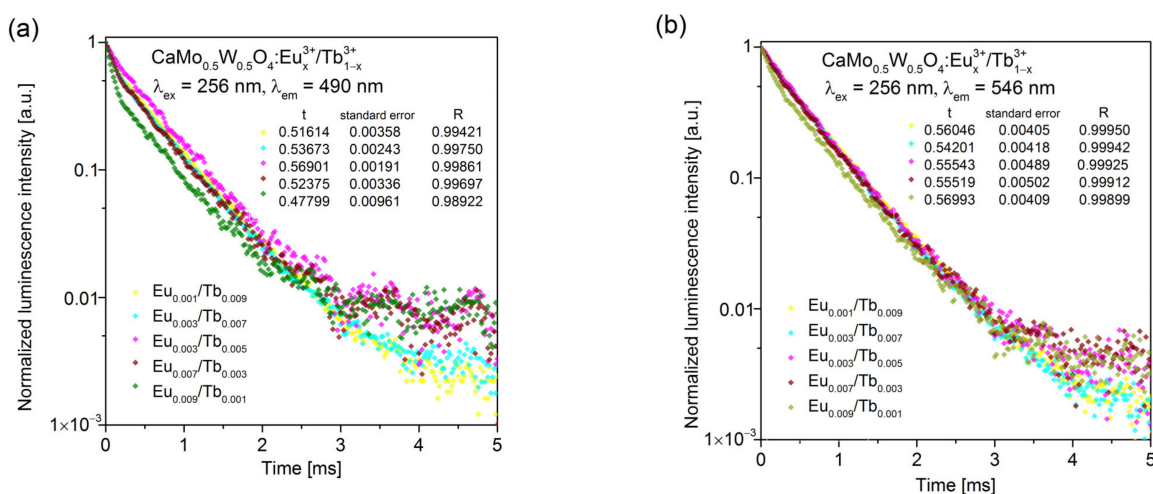


Figure 6. Cont.

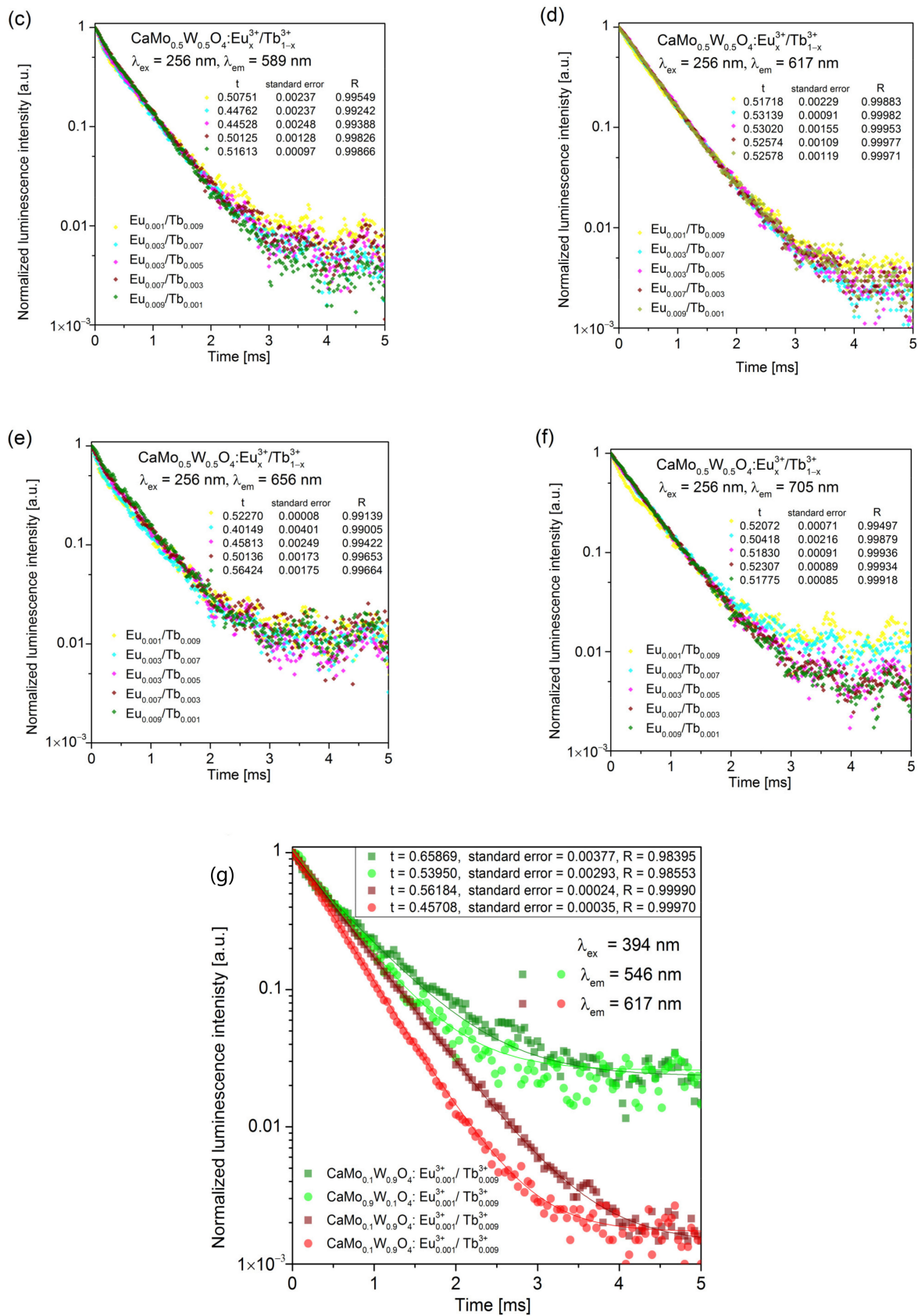
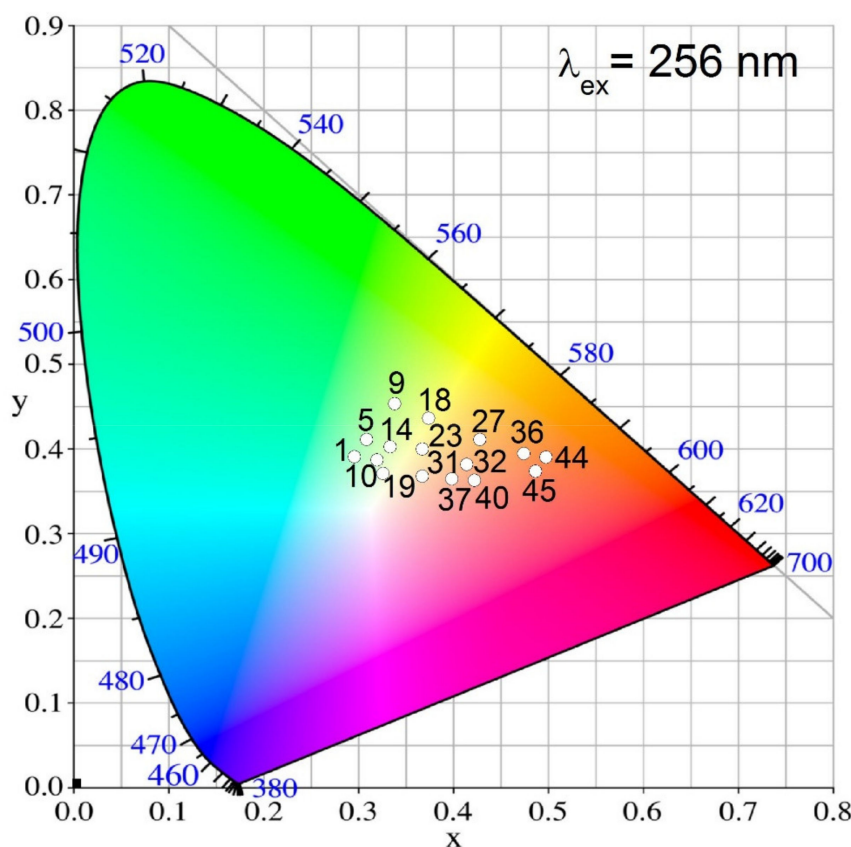


Figure 6. Luminescence decay curves for $\text{CaMo}_y\text{W}_{1-y}\text{O}_4:\text{Eu}_x^{3+}/\text{Tb}_{1-x}^{3+}$ (a) $\lambda_{\text{ex}} = 256 \text{ nm}, \lambda_{\text{em}} = 490 \text{ nm}$, (b) $\lambda_{\text{ex}} = 256 \text{ nm}, \lambda_{\text{em}} = 546 \text{ nm}$, (c) $\lambda_{\text{ex}} = 256 \text{ nm}, \lambda_{\text{em}} = 589 \text{ nm}$, (d) $\lambda_{\text{ex}} = 256 \text{ nm}, \lambda_{\text{em}} = 617 \text{ nm}$, (e) $\lambda_{\text{ex}} = 256 \text{ nm}, \lambda_{\text{em}} = 656 \text{ nm}$, (f) $\lambda_{\text{ex}} = 256 \text{ nm}, \lambda_{\text{em}} = 705 \text{ nm}$, (g) $\lambda_{\text{ex}} = 394 \text{ nm}, \lambda_{\text{em}} = 546 \text{ nm}, \lambda_{\text{em}} = 617 \text{ nm}$.

Commission International de L'Eclairage (CIE) chromaticity coordinates for $\text{CaMo}_y\text{W}_{1-y}\text{O}_4:\text{Eu}^{3+}_x/\text{Tb}^{3+}_{1-x}$ materials with different doping concentrations of Tb^{3+} and Eu^{3+} were calculated based on the corresponding emission spectra. The CIE chromaticity diagram, chromaticity coordinates, and CCT values for $\text{CaMo}_y\text{W}_{1-y}\text{O}_4:\text{Eu}^{3+}_x/\text{Tb}^{3+}_{1-x}$ excited at 256 nm are shown in Figure 7. Correlated color temperature (CCT) values were calculated using the McCamy equation [43]. We observed color shifts from yellow-green (Figure 7 sample 1, 5, Figure 8) towards the orange-red region (Figure 7 sample 44, 45, Figure 8) with an increase in the Eu^{3+} doping concentration. The CCT values are in the range of 2062–6842 K under $\lambda_{\text{ex}} = 256$ nm. Figure 7 shows the results shown for all samples series. We observed similar values for the samples No. 31 ($x = 0.3803$, $y = 0.3771$, 4007 K), 33 ($x = 0.4261$, $y = 0.3811$, 2998 K), and 34 ($x = 0.4425$, $y = 0.3839$, 2735 K) with the main colorimetric data of the LED illuminator V2 ($x = 0.3781$, $y = 0.3775$, 4070 K), B2 ($x = 0.4357$, $y = 0.4012$, 2988 K), and B1 ($x = 0.4560$, $y = 0.4078$, 2773 K), respectively, recommended by CIE [49]. Figure 8 shows pictures of $\text{CaMo}_y\text{W}_{1-y}\text{O}_4:\text{Eu}^{3+}_x/\text{Tb}^{3+}_{1-x}$ under UV light in Eppendorf tubes and glass tubes.



samples	x	y	CCT [K]
1.	0.2960	0.3898	6842
2.	0.2946	0.3987	6836
3.	0.3039	0.4077	6444
4.	0.2972	0.3926	6776
5.	0.3087	0.4104	6268
6.	0.3210	0.4420	5818
7.	0.3329	0.4621	5495
8.	0.3448	0.4470	5189
9.	0.3384	0.4524	5354
10.	0.3198	0.3860	5949
11.	0.3324	0.3930	5504
12.	0.3500	0.4040	4975
13.	0.3346	0.3987	5434
14.	0.3336	0.4018	5466
15.	0.3612	0.4153	4701
16.	0.3741	0.4246	4417
17.	0.3635	0.4232	4669
18.	0.3740	0.4353	4462
19.	0.3258	0.3701	5752
20.	0.3341	0.3881	5446
21.	0.3660	0.3930	4486
22.	0.3573	0.3895	4720
23.	0.3673	0.3992	4479
24.	0.3884	0.4015	3961
25.	0.4092	0.4041	3522
26.	0.4477	0.3991	2785
27.	0.4276	0.4101	3213
28.	0.3675	0.3671	4308
29.	0.3911	0.3812	3759
30.	0.3875	0.3827	3859
31.	0.3803	0.3771	4007
32.	0.4137	0.3808	3242
33.	0.4261	0.3811	2998
34.	0.4425	0.3839	2735
35.	0.4283	0.4042	3154
36.	0.4740	0.3938	2372
37.	0.3983	0.3638	3438
38.	0.4029	0.3679	3366
39.	0.4158	0.3612	3013
40.	0.4218	0.3620	2898
41.	0.4598	0.3674	2320
42.	0.4488	0.3658	2462
43.	0.4607	0.3707	2339
44.	0.4973	0.3893	2086
45.	0.4862	0.3727	2062

Figure 7. CIE chromaticity diagram, chromaticity coordinates, and correlated color temperature (CCT) of all phosphors of the $\text{CaMo}_y\text{W}_{1-y}\text{O}_4:\text{Eu}^{3+}_x/\text{Tb}^{3+}_{1-x}$ series excited at 256 nm: series 1–9: $\text{Eu}^{3+}_{0.001}/\text{Tb}^{3+}_{0.009}\text{Mo}_{(0.1-0.9)}\text{W}_{(0.9-0.1)}$, series 10–18: $\text{Eu}^{3+}_{0.003}/\text{Tb}^{3+}_{0.007}\text{Mo}_{(0.1-0.9)}\text{W}_{(0.9-0.1)}$, series 19–27: $\text{Eu}^{3+}_{0.005}/\text{Tb}^{3+}_{0.005}\text{Mo}_{(0.1-0.9)}\text{W}_{(0.9-0.1)}$, series 28–36: $\text{Eu}^{3+}_{0.007}/\text{Tb}^{3+}_{0.003}\text{Mo}_{(0.1-0.9)}\text{W}_{(0.9-0.1)}$, series 37–45: $\text{Eu}^{3+}_{0.009}/\text{Tb}^{3+}_{0.001}\text{Mo}_{(0.1-0.9)}\text{W}_{(0.9-0.1)}$.

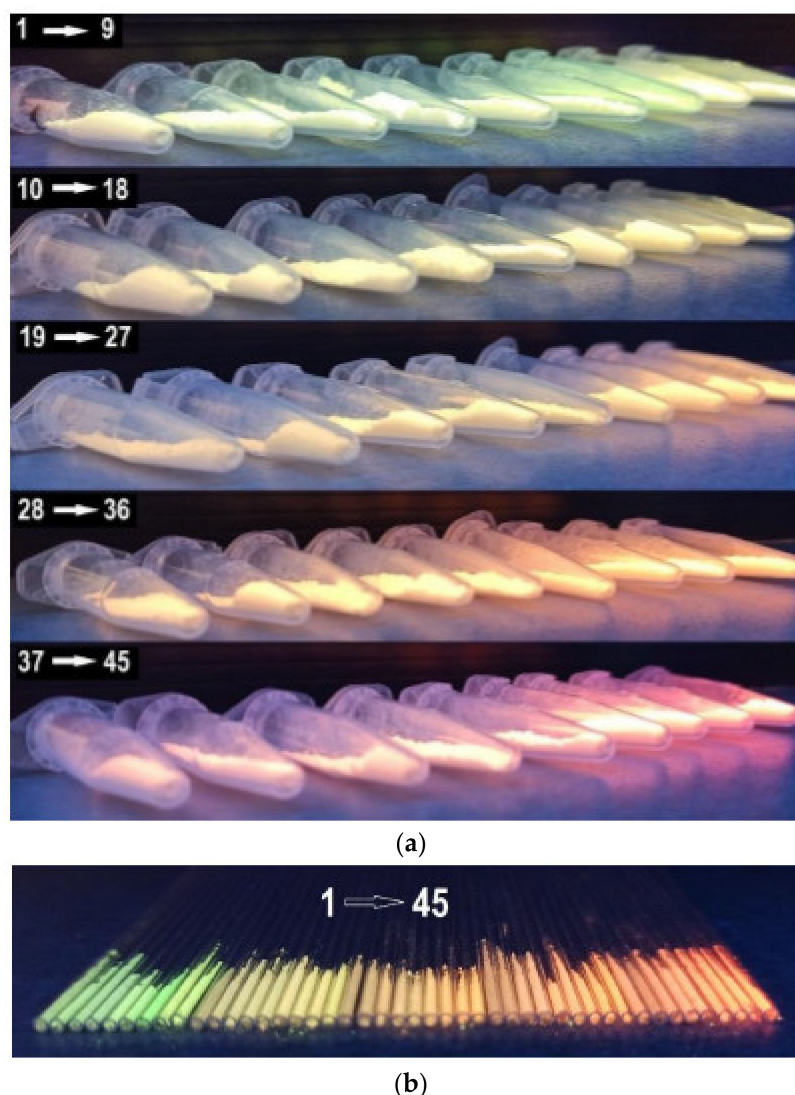


Figure 8. Images of $\text{CaMo}_y\text{W}_{1-y}\text{O}_4:\text{Eu}^{3+}_x/\text{Tb}^{3+}_{1-x}$ under UV in (a) Eppendorf tubes and (b) glass tubes.

4. Conclusions

In summary, multicolor molybdate–tungstate microphosphors co-doped with Tb^{3+} and Eu^{3+} were synthesized successfully using the high temperature solid state method. XRD analysis shows that the synthesized phosphors are single-phase with a tetragonal $I4_1/a$ structure. The excitation spectra show a charge transfer band between 200 and 350 nm which effectively activates the emissions of Eu^{3+} and Tb^{3+} ions through energy transfer between WO_4^{3-} and MoO_4^{3-} groups and activator ions, after CT between W^{6+} or Mo^{6+} and O^{2-} . Scanning electron microscopy (SEM) images presented a strong tendency for phosphors to agglomerate, which is specific to the high temperature solid state synthesis method we used. At 265 nm excitation, the $\text{CaMo}_y\text{W}_{1-y}\text{O}_4:\text{Eu}^{3+}_x/\text{Tb}^{3+}_{1-x}$ microphosphors show color shifts from yellow-green to orange-red with an increasing doping concentration of Eu^{3+} . The intense emission upon UV light excitation indicates that the new multicolored tungstate–molybdate microphosphors can be used as an alternative to LED components. Detailed studies of $\text{Eu}^{3+}/\text{Tb}^{3+}$ -doped phosphors based on the mixed molybdate–tungstate matrix, whose luminescent properties were controlled by the composition of the matrix and the number of doping ions, showed that the obtained values of correlated color temperature (CCT) and chromaticity parameters were similar to those recommended by CIE. In addition, the use of a relatively small number of doping ions, compared to others described in the

literature, allows for intense emission of the tested phosphors, which is important from an economic point of view.

Author Contributions: Conceptualization, methodology, formal analysis, visualization, writing-original draft preparation J.C.; writing-review and editing, supervision, A.S.; review and editing N.K.; writing-review and editing S.L. All authors have read and agreed to the published version of the manuscript.

Funding: This research received no external funding.

Institutional Review Board Statement: Not applicable.

Informed Consent Statement: Not applicable.

Data Availability Statement: Data sharing not applicable.

Conflicts of Interest: The authors declare no conflict of interest.

References

- Mahalingam, V.; Thirumalai, J.; Krishnan, R.; Chandramohan, R. Controlled synthesis and luminescence properties of $\text{Ca}_{0.5}\text{Y}_{1-x}(\text{MoO}_4)_2 \cdot x\text{RE}^{3+}$ (RE = Eu, Pr, Sm, Tb, Dy, Yb/Er, Yb/Tm, and Yb/Ho) phosphors by hydrothermal method versus pulsed laser deposition. *Electron. Mater. Lett.* **2016**, *12*, 32–47. [[CrossRef](#)]
- Lim, C.S.; Atuchin, V.V.; Aleksandrovsky, A.S.; Molokeev, M.S.; Oreshonkov, A.S. Incommensurately modulated structure and spectroscopic properties of $\text{CaGd}_2(\text{MoO}_4)_4$: $\text{Ho}^{3+}/\text{Yb}^{3+}$ phosphors for up-conversion applications. *J. Alloys Compd.* **2016**, *695*, 737–746. [[CrossRef](#)]
- Tranquilin, R.L.; Oliveira, M.C.; Santiago, A.A.G.; Lovisa, L.X.; Ribeiro, R.A.P.; Longo, E.; de Lazaro, S.R.; Almeida, C.R.R.; Paskocimas, C.A.; Motta, F.V.; et al. Presence of excited electronic states on terbium incorporation in CaMoO_4 : Insights from experimental synthesis and first-principles calculations. *J. Phys. Chem Solids.* **2021**, *149*, 109790. [[CrossRef](#)]
- Zhou, Y.; He, X.H.; Yan, B. Self-assembled $\text{RE}_2(\text{MO}_4)_3$: Ln^{3+} (RE = Y, La, Gd, Lu; M = W, Mo; Ln = Yb/Er, Yb/Tm) hierarchical microcrystals: Hydrothermal synthesis and up-conversion luminescence. *Opt Mater.* **2014**, *36*, 602–607. [[CrossRef](#)]
- Lim, C.S. Microwave Sol-Gel Derived $\text{NaGd}(\text{MoO}_4)_2$: $\text{Ho}^{3+}/\text{Yb}^{3+}$ Phosphors and Their Upconversion Photoluminescence Properties. *Trans. Electr. Electron. Mater.* **2017**, *18*, 364–369.
- Xia, M.; Ju, Z.; Yang, H.; Wang, Z.; Gao, X.; Pan, F.; Liu, W. Red-emitting enhancement by inducing lower crystal field symmetry of Eu^{3+} site in CaWO_4 : Eu^{3+} phosphor for n-UV w-LEDs. *J. Alloys Compd.* **2018**, *739*, 439–446. [[CrossRef](#)]
- Zhang, W.; Zhang, R.; Yang, S.; Wang, R.; Na, L.; Hua, R. Synthesis and photoluminescent features of Eu^{3+} -doped $\text{NaGd}(\text{WO}_4)_2$ nanophosphors. *Mater. Res. Bull.* **2020**, *122*, 110689. [[CrossRef](#)]
- Teymouri, E.; Alemi, A.; Aghdam sharabiyani, M.A.; Sadeghi, L.; Necefoglu, H. Synthesizes and characterization of new double tungstate $\text{NaRE}(\text{WO}_4)_2$ (RE = Pr^{3+} , Ho^{3+} , Sm^{3+}). *Mater. Chem. Phys.* **2020**, *240*, 122173. [[CrossRef](#)]
- Cavalli, E.; Boutinaud, P.; Grinberg, M. Luminescence dynamics in CaWO_4 : Pr^{3+} powders and single crystals. *J. Lumin.* **2016**, *169*, 450–453. [[CrossRef](#)]
- Kubus, M.; Klonowski, A.M.; Lotnyk, A.; Kienle, L. Luminescence enhancement in composite material: CaWO_4 : Tb^{3+} nanocrystals incorporated into silica xerogel. *Mater. Chem. Phys.* **2015**, *150*, 424–429. [[CrossRef](#)]
- Dudnikova, V.B.; Zharikov, E.V.; Eremin, N.N. Local structure of molybdates solid solutions containing europium by results of atomistic simulation. *Mater. Today Commun.* **2020**, *23*, 101180. [[CrossRef](#)]
- Subbotin, K.A.; Titov, A.I.; Lis, D.A.; Smirnov, V.A.; Alimov, O.K.; Zharikov, E.V.; Shcherbakov, I.A. Downconversion properties of Yb-doped scheelitelike molybdate and tungstate single crystals. In Proceedings of the International Conference Laser Optics (ICLO), St. Petersburg, Russia, 4–8 June 2018; p. 331. [[CrossRef](#)]
- You, C.Y.; Colon, C.; Fernandez-Martinez, F.; De Andre-Garcia, I. Synthesis and characterization of a Ce^{3+} trivalent scheelite-type double tungstate by solid state method. *J. Alloys Compd.* **2017**, *694*, 345–353. [[CrossRef](#)]
- Culver, S.P.; Brutchey, R.L. Lanthanide-activated scheelite nanocrystal phosphors prepared by the low-temperature vapor diffusion sol-gel method. *Dalt. Trans.* **2016**, *45*, 18069–18073. [[CrossRef](#)] [[PubMed](#)]
- Nadaraia, L.; Jalabadze, N.; Chedia, R.; Antadze, M.; Khundadze, L. Preparation of Tungstate nanopowders by Sol-Gel method. *IEEE Trans. Nucl. Sci.* **2010**, *57*, 1370–1376. [[CrossRef](#)]
- Yang, L.; Wang, Y.; Wang, Y.; Wang, X.; Han, G. Shape-controlled of CaWO_4 microcrystals by self-assembly of nanocrystals via a simple sonochemical method. *Adv. Powder Technol.* **2013**, *24*, 721–726. [[CrossRef](#)]
- De Sousa, P.B.; Gouveia, A.F.; Sczancoski, J.C.; Nogueira, I.C.; Longo, E.; San-Miguel, M.A.; Cavalcante, L.S. Electronic structure, optical and sonophotocatalytic properties of spindle-like CaWO_4 microcrystals synthesized by the sonochemical method. *J. Alloys Compd.* **2021**, *855*, 157377. [[CrossRef](#)]
- Tang, Y.; Ye, Y.; Liu, H.; Guo, X.; Tang, H.; Yin, W.; Gao, Y. Hydrothermal synthesis of $\text{NaLa}(\text{WO}_4)_2$: Eu^{3+} octahedrons and tunable luminescence by changing Eu^{3+} concentration and excitation wavelength. *J. Mater. Sci Mater. Electron.* **2017**, *28*, 1301–1306. [[CrossRef](#)]

19. Czajka, J.; Szczeszak, A.; Lis, S. Up-converting nanophosphors based on Yb³⁺/Ho³⁺ doped NaM (WO₄)₂ (M = Gd, Y) synthesized in situ under hydrothermal conditions. *Opt Mater.* **2020**, *107*, 109979. [[CrossRef](#)]
20. Xiang, S.; Chen, B.; Zhang, J.; Li, X.; Sun, J.; Zheng, H.; Wu, Z.; Zhong, H.; Yu, H.; Xia, H. Microwave-assisted hydrothermal synthesis and laser-induced optical heating effect of NaY (WO₄)₂: Tm³⁺/Yb³⁺ microstructures. *Opt. Mater. Express.* **2014**, *4*, 1966–1980. [[CrossRef](#)]
21. Zheng, H.; Chen, B.; Yu, H.; Zhang, J.; Sun, J.; Li, X.; Sun, M.; Tian, B.; Fu, S.; Zhong, H.; et al. Microwave-assisted hydrothermal synthesis and temperature sensing application of Er³⁺/Yb³⁺ doped NaY (WO₄)₂ microstructures. *J. Colloid. Interface Sci.* **2014**, *420*, 27–34. [[CrossRef](#)]
22. Czajka, J.; Piskula, Z.; Szczeszak, A.; Lis, S. Structural, morphology and luminescence properties of mixed calcium molybdate-tungstate microcrystals doped with Eu³⁺ ions and changes of the color emission chromaticity. *Opt Mater.* **2018**, *84*, 422–426. [[CrossRef](#)]
23. Zhang, S.; Lv, L.; Wang, H.; Zhu, C.; Pang, R.; Feng, J.; Li, D.; Liu, G.; Jiang, L.; Li, C. Structure and luminescence properties of CaWO₄-EuMO₄ (M=Nb, Ta) solid solution. *J. Lumin.* **2019**, *211*, 183–192. [[CrossRef](#)]
24. Huang, X.; Li, B.; Guo, H.; Chen, D. Molybdenum-doping-induced photoluminescence enhancement in Eu³⁺-activated CaWO₄ red-emitting phosphors for white light-emitting diodes. *Dye Pigment.* **2017**, *143*, 86–94. [[CrossRef](#)]
25. Wang, H.; Yang, T.; Feng, L.; Ning, Z.; Liu, M.; Lai, X.; Gao, D.; Bi, J. Energy Transfer and Multicolor Tunable Luminescence Properties of NaGd_{0.5}Tb_{0.5-x}Eu_x (MoO₄)₂ Phosphors for UV-LED. *J. Electron. Mater.* **2018**, *47*, 6494–6506. [[CrossRef](#)]
26. Atuchin, V.V.; Grossman, V.G.; Adichtchev, S.V.; Surovtsev, N.V.; Gavrilova, T.A.; Bazarov, B.G. Structural and vibrational properties of microcrystalline TIM (MoO₄)₂ (M = Nd, Pr) molybdates. *Opt. Mater.* **2012**, *34*, 812–816. [[CrossRef](#)]
27. Wang, Y.; Hong, F.; Yu, L.; Xu, H.; Liu, G.; Dong, X.; Yu, W.; Wu, J. Construction, energy transfer, tunable multicolor and luminescence enhancement of YF₃:RE³⁺ (RE=Eu, Tb)/carbon dots nanocomposites. *J. Lumin.* **2020**, *221*, 117072. [[CrossRef](#)]
28. Kataria, V.; Mehta, D.S. Multispectral harvesting rare-earth oxysulphide based highly efficient transparent luminescent solar concentrator. *J. Rare Earths* **2021**. [[CrossRef](#)]
29. Sarkar, J.; Mondal, S.; Panja, S.; Dey, I.; Sarkar, A.; Ghorai, U.K. Multicolour tuning and perfect white emission from novel PbWO₄:Yb³⁺: Ho³⁺: Tm³⁺ nanophosphor. *Mater. Res. Bull.* **2019**, *112*, 314–322. [[CrossRef](#)]
30. Sun, Z.; Jiang, L.; Xu, X.; Li, J.; Chen, X.; Chen, H. Synthesis and Luminescence Properties of Ho³⁺ and Er³⁺-Doped CaWO₄ Nanocrystalline Powders Prepared by Self-Propagating Combustion Method. *J. Fluoresc.* **2020**, *30*, 389–396. [[CrossRef](#)]
31. Wang, Z.; Liang, H.; Wang, Q.; Luo, L.; Gong, M. Luminescent properties of Tb³⁺ activated double molybdates and tungstates. *Mater. Sci. Eng. B Solid State Mater. Adv. Technol.* **2009**, *164*, 120–123. [[CrossRef](#)]
32. Bawane, U.A.; Kadam, A.R.; Nande, A.; Dhoble, S.J. Critical review on lanthanide activated LED phosphors. *J. Phys. Conf. Ser.* **2021**, *1913*, 012030. [[CrossRef](#)]
33. Song, F. Synthesis and photoluminescence of new Eu³⁺-activated Cs₂Ba (MoO₄)₂ red-emitting phosphors with high color purity for white LEDs. *J. Lumin.* **2020**, *239*, 118324. [[CrossRef](#)]
34. Li, J.; Liu, X.; Liu, Y. Luminescence investigation of a novel red-emitting Sr₃NaSbO₆: Eu³⁺ phosphor. *Optik* **2021**, *242*, 166809. [[CrossRef](#)]
35. Zhou, Y.X.; Yi, S.; Fang, Z.X.; Lu, J.; Hu, Z.; Zhao, W.; Wang, Y. Research on a new type of near-infrared phosphor Li₂MgZrO₄:Cr³⁺ synthesis, crystal structure, photoluminescence and thermal stability. *Opt. Mater.* **2021**, *117*, 111209. [[CrossRef](#)]
36. Rodríguez-García, M.M.; Ciric, A.; Ristic, Z.; Williams, J.A.G.; Dramićanin, M.D.; Evans, I.R. Narrow-band red phosphors of high colour purity based on Eu³⁺-activated apatite-type Gd_{9.33} (SiO₄)₆O₂. *J. Mater. Chem. C.* **2021**, *9*, 7474. [[CrossRef](#)]
37. Sahu, M.; Phatak, N.; Saxena, M.K. Exploring color tunable emission characteristics of Eu³⁺-doped La₂ (MoO₄)₃ phosphors in the glass-ceramic form. *RSC Adv.* **2021**, *11*, 17488. [[CrossRef](#)]
38. Perera, S.S.; Munasinghe, H.N.; Yatooma, E.N.; Rabuffe, F.A. Microwave-assisted solid-state synthesis of NaRE (MO₄)₂ phosphors (RE = La, Pr, Eu, Dy; M = Mo, W). *Dalton Trans.* **2020**, *49*, 7914–7919. [[CrossRef](#)]
39. Bin, J.; Liu, H.; Mei, L.; Liang, L.; Gao, H.; Li, H.; Liao, L. Multi-color Luminescence Evolution and Efficient Energy Transfer of Scheelite-type LiCaGd (WO₄)₃: Ln³⁺ (Ln = Eu, Dy, Tb) Phosphors. *Ceram. Int.* **2019**, *45*, 1837–1845. [[CrossRef](#)]
40. Guo, X.; Song, S.; Jiang, X.; Cui, J.; Li, Y.; Lv, W.; Liu, H.; Han, Y.; Wang, L. Functional applications and luminescence properties of emission tunable phosphors CaMoO₄@SiO₂:Ln³⁺ (Ln=Eu, Tb, Dy). *J. Alloys Compd.* **2021**, *857*, 157515. [[CrossRef](#)]
41. Wang, C.; Zhou, T.; Jiang, J.; Geng, H.; Ning, Z.; Lai, X.; Bi, J.; Gao, D. Multicolor Tunable Luminescence Based on Tb³⁺/Eu³⁺ Doping through a Facile Hydrothermal Route. *ACS Appl. Mater. Interfaces* **2017**, *9*, 26184–26190. [[CrossRef](#)]
42. Vijayalakshmi, L.; Kumar, K.N.; Hwang, P. Tailoring ultraviolet-green to white light via energy transfer from Tb³⁺-Eu³⁺ codoped glasses for white light-emitting diodes. *Scr. Mater.* **2020**, *187*, 97–102. [[CrossRef](#)]
43. McCamy, C.S. Correlated color temperature as an explicit function of chromaticity coordinates. *Color. Res. Appl.* **1992**, *17*, 142–144. [[CrossRef](#)]
44. Zhao, Y.; Wang, X.; Zhang, Y.; Li, Y.; Yao, X. Winning wide-temperature-range and high-sensitive thermometry by a multichannel strategy of dual-lanthanides in the new tungstate phosphors. *J. Alloys Compd.* **2020**, *834*, 154998. [[CrossRef](#)]
45. Gürmen, E.; Daniels, E.; King, J.S. Crystal Structure Refinement of SrMoO₄, SrWO₄, CaMoO₄, and BaWO₄ by Neutron Diffraction. *J. Chem. Phys.* **1971**, *55*, 1093–1097. [[CrossRef](#)]
46. Piskula, Z.; Staninski, K.; Lis, S. Luminescence properties of Tm³⁺/Yb³⁺, Er³⁺/Yb³⁺ and Ho³⁺/Yb³⁺ activated calcium tungstate. *J. Rare Earths.* **2011**, *29*, 1166–1169. [[CrossRef](#)]

-
47. Li, S.; Wei, X.; Deng, K.; Tian, X.; Qin, Y.; Chen, Y.; Yin, M. A new red-emitting phosphor of Eu^{3+} -doped $\text{Sr}_2\text{MgMo}_x\text{W}_{1-x}\text{O}_6$ for solid state lighting. *Curr. Appl. Phys.* **2013**, *13*, 1288–1291. [[CrossRef](#)]
 48. Jiang, H.-X.; Lǚ, S.-C. White light emission and bidirectional energy transfer in a $\text{Eu}^{3+}/\text{Tb}^{3+}$ co-doped $\text{NaLa}(\text{WO}_4)_2$. *Mater. Res. Bull.* **2020**, *135*, 11123. [[CrossRef](#)]
 49. Martínez-Domingo, M.Á.; Melgosa, M.; Okajima, K.; Medina, V.J.; Collado-Montero, F.J. Spectral Image Processing for Museum Lighting Using CIE LED Illuminants. *Sensors* **2019**, *19*, 5400. [[CrossRef](#)]